

The natural frequencies of the resting human brain: An MEG-based atlas

Almudena Capilla^{a,*}, Lydia Arana^a, Marta García-Huésca^a, María Melcón^a, Joachim Gross^b, Pablo Campo^c

^a Departamento de Psicología Biológica y de la Salud, Facultad de Psicología, Universidad Autónoma de Madrid, Madrid 28049, Spain

^b Institute for Biomagnetism and Biosignal Analysis, University of Münster, Münster, Germany

^c Departamento de Psicología Básica, Facultad de Psicología, Universidad Autónoma de Madrid, Madrid 28049, Spain

ARTICLE INFO

Keywords:

Brain oscillations
Clustering
Human
Magnetoencephalography
Resting state
Spectral analysis

ABSTRACT

Brain oscillations are considered to play a pivotal role in neural communication. However, detailed information regarding the typical oscillatory patterns of individual brain regions is surprisingly scarce. In this study we applied a multivariate data-driven approach to create an atlas of the natural frequencies of the resting human brain on a voxel-by-voxel basis. We analysed resting-state magnetoencephalography (MEG) data from 128 healthy adult volunteers obtained from the Open MEG Archive (OMEGA). Spectral power was computed in source space in 500 ms steps for 82 frequency bins logarithmically spaced from 1.7 to 99.5 Hz. We then applied k-means clustering to detect characteristic spectral profiles and to eventually identify the natural frequency of each voxel. Our results provided empirical confirmation of the canonical frequency bands and revealed a region-specific organisation of intrinsic oscillatory activity, following both a medial-to-lateral and a posterior-to-anterior gradient of increasing frequency. In particular, medial fronto-temporal regions were characterised by slow rhythms (delta/theta). Posterior regions presented natural frequencies in the alpha band, although with differentiated generators in the precuneus and in sensory-specific cortices (i.e., visual and auditory). Somatomotor regions were distinguished by the mu rhythm, while the lateral prefrontal cortex was characterised by oscillations in the high beta range (>20 Hz). Importantly, the brain map of natural frequencies was highly replicable in two independent subsamples of individuals. To the best of our knowledge, this is the most comprehensive atlas of ongoing oscillatory activity performed to date. Critically, the identification of natural frequencies is a fundamental step towards a better understanding of the functional architecture of the human brain.

1. Introduction

Electrophysiological brain activity is currently understood as a combination of aperiodic (1/f-like) and periodic oscillatory components (Donoghue et al., 2020) that are spontaneously generated at rest and can be captured by means of electro- and magnetoencephalography (EEG/MEG) (for a review see Lopes da Silva, 2013). Critically, brain oscillations are considered to be at the basis of the communication code between neural networks (Buzsáki & Watson, 2012; Fries, 2015; Varela et al., 2001). Hence, characterising the typical patterns of oscillatory activity is crucial for understanding the functional architecture of the brain that is at the core of perception, cognition, and behaviour.

Since Jasper and Penfield (1949) first attempts, several studies have tried to establish common oscillatory patterns across the resting human brain. Overall, oscillations at alpha frequency (8–13 Hz) are consistently found over occipital areas, theta-band activity (4–8 Hz) over frontal regions, and beta (13–30 Hz) and mu rhythms (characterised

by spectral peaks in the alpha and beta ranges) around perirolandic areas, whereas delta (0.5–4 Hz) and gamma-band oscillations (>30 Hz) are found to be less conspicuous and not always localized to the same regions (Chen et al., 2008; Congedo et al., 2010; Groppe et al., 2013; Hillebrand et al., 2012; Lew et al., 2021; Mahjoory et al., 2020; Niso et al., 2016; Niso et al., 2019; Ramkumar et al., 2014).

However, beyond this general description, information regarding the characteristic oscillatory activity of individual brain regions is surprisingly scarce. Two approaches have been employed in order to achieve this aim. First, typical rhythmic patterns at specific brain locations have recently been inferred from both intracranial EEG (iEEG; Frauscher et al., 2018; Kalamangalam et al., 2020) and MEG recordings (Keitel & Gross, 2016; Mellem et al., 2017). These studies have provided the first detailed maps of ongoing rhythmic activity throughout the brain. However, a common methodological constraint is the use of predefined frequency bands and/or regions of interest. While it is a common practice to classify oscillatory activity into bands, this is not optimal since the borders between canonical frequency ranges have been

Abbreviations: MEG, Magnetoencephalography.

* Corresponding author.

E-mail address: almudena.capilla@uam.es (A. Capilla).

<https://doi.org/10.1016/j.neuroimage.2022.119373>.

Received 12 January 2022; Received in revised form 2 June 2022; Accepted 10 June 2022

Available online 11 June 2022.

1053-8119/© 2022 The Authors. Published by Elsevier Inc. This is an open access article under the CC BY-NC-ND license (<http://creativecommons.org/licenses/by-nc-nd/4.0/>)

arbitrarily drawn and, consequently, oscillations arising from the same physiological machinery in different species, at different ages, or even in the same individual across states are often labelled as different rhythms (Boersma et al., 2011; Buzsáki, 2006; Buzsáki et al., 2013). Similarly, in most studies the brain is parcellated into predefined regions of interest based on an anatomical atlas, which does not necessarily have to overlap with the organisation of the brain based on its functional properties (Eickhoff et al., 2018).

An alternative approach to mapping region-specific spectral patterns is based on direct perturbation of intrinsic oscillations. The stimulation of a specific cortical location by a single pulse of transcranial magnetic stimulation (TMS) evokes an oscillatory response that can be detected by concurrent EEG recordings (Ferrarelli et al., 2012; Rosanova et al., 2009). The main frequency of the evoked response is referred to as the ‘natural’ frequency and indicates the preferred rate at which the targeted cortical region is intrinsically tuned to oscillate (Basar, 1992; Rosanova et al., 2009). These studies have accurately detected natural frequencies within the alpha range in the occipital cortex, low beta-band responses in parietal and periorolandic areas, and high beta-band oscillations in the prefrontal cortex (Ferrarelli et al., 2012; Rosanova et al., 2009). Since TMS stimulation is restricted to few locations, Amengual et al. (2019) have recently tried to develop a finer-grained atlas of natural frequencies by applying single pulses of intracranial electrical stimulation while recording iEEG in epileptic patients. Although this is a promising tool, the positioning of electrodes is constrained by clinical criteria for ethical reasons, resulting in some regions being over-sampled (e.g., temporal lobe), while others are under-sampled.

The present study aimed to address the limitations of previous research to create a detailed normative atlas of the natural frequencies of the resting human brain. Natural frequency in this context could be defined as the peak frequency of the most characteristic spectral pattern of a brain region in comparison with others. To further characterise the brain’s intrinsic rhythmic activity, we additionally identified the ‘dominant’ frequencies, i.e., the predominant oscillatory frequency of a brain region. A non-invasive strategy was employed to detect distinctive spectral patterns in a large sample of healthy individuals from a previously recorded MEG dataset. To avoid an *a priori* definition of frequency ranges and regions of interest, we applied a multivariate data-driven approach whereby exact natural frequencies were identified on a voxel-by-voxel basis.

2. Material and methods

2.1. Participants and data acquisition

Data were downloaded from the OMEGA database (Niso et al., 2016), which provides open access to anonymised resting state MEG data and anatomical T1-weighted Magnetic Resonance Images (MRIs). Brain activity was acquired with a whole-head CTF MEG system at the Montreal Neurological Institute (MNI, McGill University). MEG data were recorded in a magnetically shielded room with 275 axial gradiometers and 26 MEG reference sensors at a 2400 Hz sampling rate. An anti-aliasing low-pass filter at 600 Hz and CTF third-order gradient compensation were applied online. Electrooculography (EOG) and electrocardiography (ECG) recordings were also obtained. In addition, individual head shapes and three anatomical landmarks (nasion, left- and right- pre-auricular points) were digitised to facilitate MEG-MRI co-registration. Data collection and analysis were approved by the institutional ethics committees and conducted in compliance with the declaration of Helsinki.

MEG recordings were collected from participants while sitting upright. They were asked to stay awake and keep their eyes open on a fixation cross for 5 minutes. We analysed data from 128 healthy volunteers (68 males, 118 right-handed, mean age 30.5 ± 12.4 [M \pm SD]

years, age range 19–73 years). We only used data from one recording session per participant.

2.2. Pre-processing

Data analysis was conducted with FieldTrip (version 20180405; Oostenveld et al., 2011) and in-house Matlab code. All scripts necessary to reproduce the analysis and the figures in this paper are available at <https://github.com/necog-UAM/OMEGA-NaturalFrequencies>. MEG signals were first denoised by applying Principal Component Analysis (PCA) on the reference sensors. Then, we applied a third-order Butterworth high-pass filter with a cut-off frequency of 0.05 Hz to remove slow fluctuations. Power line noise at 60 Hz, and harmonics at 120 and 180 Hz were reduced via spectrum interpolation (Leske & Dalal, 2019). Finally, the MEG signal was demeaned, detrended, and resampled at 512 Hz.

Artifact correction was performed using Independent Component Analysis (ICA), following a PCA-based dimensionality reduction to 40 components. ICs reflecting cardiac, ocular, or muscular activity were identified and projected out of the MEG signal. The data were visually inspected for any remaining artifacts. Contaminated data segments were excluded from further analysis.

2.3. Reconstruction of source-level activity

The T1-weighted MRI of each individual was co-registered to the MEG head coordinate space by means of a semi-automatic procedure. An initial alignment was obtained by manually locating three anatomical landmarks (nasion, left- and right- pre-auricular points) in the MRI. We then employed a modified version of the Iterative Closest Point algorithm (Besl & McKay, 1992) to automatically fit the digitised head shape onto the scalp surface extracted from the participant’s MRI.

The forward model was computed using a realistic single shell volume conductor model (Nolte, 2003). We adapted a MNI-standard grid of 1-cm resolution to each individual’s brain volume and compute the lead fields for every voxel. Only voxels located within the cerebral cortex and hippocampus were considered.

Source-level time series were then reconstructed using linearly constrained minimum variance beamforming (LCMV; Van Veen et al., 1997). We employed the covariance of the artifact-free data to compute the spatial filter weights with the regularization parameter lambda set to 10%. Beamforming weights were subsequently used to estimate source-space time series from sensor-level data (Fig. 1A).

2.4. Frequency analysis on source-level data

Frequency analysis was conducted on the reconstructed source-space signal. We applied a Hanning-tapered sliding window Fourier transform moving in steps of 500 ms. Oscillatory power was computed for 82 frequency bins logarithmically spaced from 1.7 to 99.5 Hz. We used a frequency-dependent window width set to 5 cycles per time window, which attenuated the 1/f aperiodic component of the signal and highlighted periodic oscillatory activity. To check that the selected number of cycles did not influence the results, we performed additional analyses for 3 and 7 cycles per time window. In addition, to avoid edge effects, we discarded 5.8-s time intervals (i.e., 10 cycles of the lowest frequency) at the beginning and end of every artifact-free data segment. As a result, we obtained a set of 505 ± 59 power spectra per voxel and participant, each containing the frequency components of the signal at a given time instant. Finally, in order to account for the center of the head bias, each spectrum was expressed as relative power by dividing the power at each frequency by the absolute power summed over the whole spectrum (Fig. 1B).

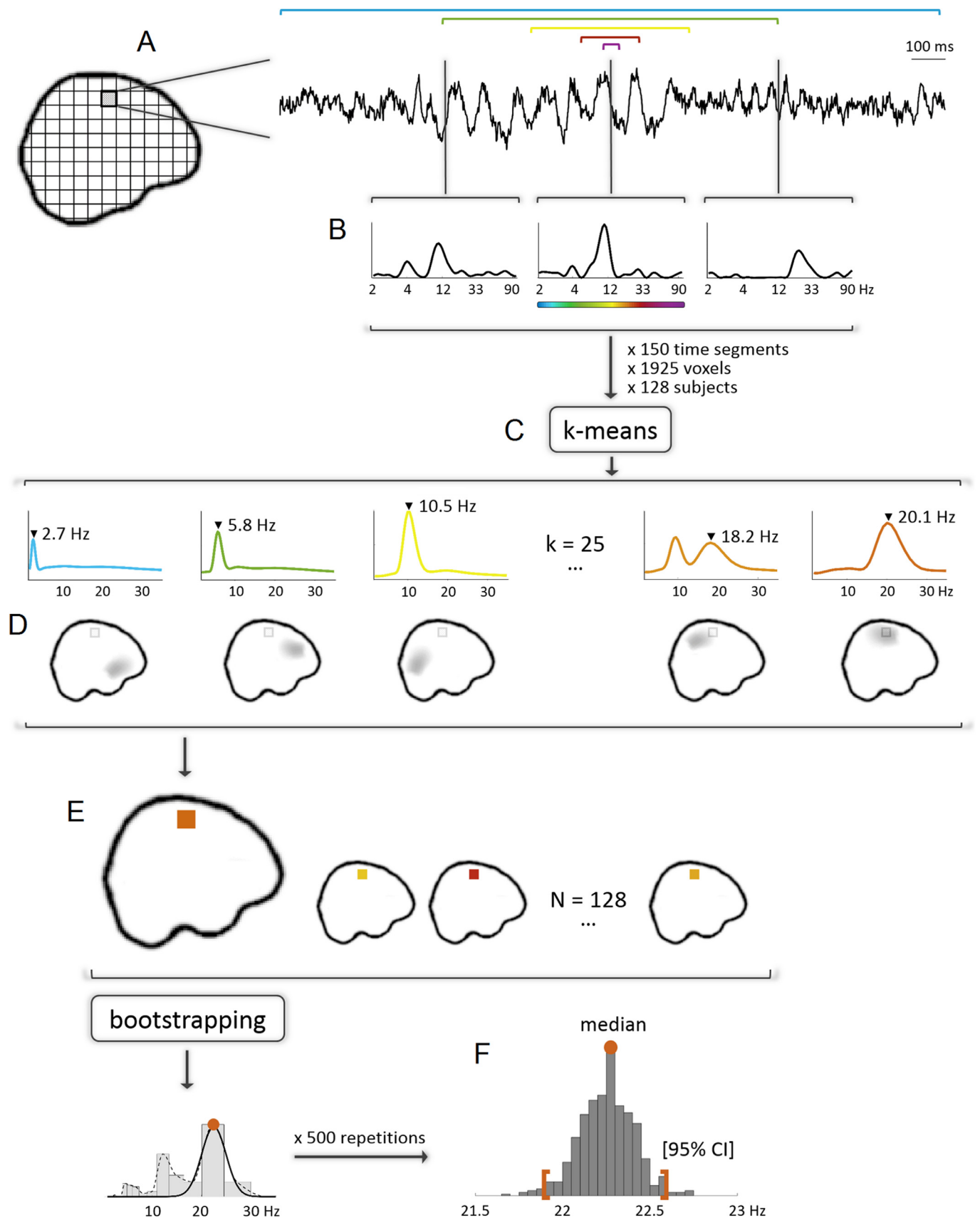


Fig. 1. Methodological pipeline for obtaining the brain atlas of natural frequencies. (A) Beamforming reconstruction of source-level time series. (B) Spectral analysis of source-level data using a frequency-dependent window width of 5 cycles per frequency. (C) K-means clustering ($k = 25$) of source-space power spectra computed for 150 time segments \times 1925 voxels \times 128 subjects. (D) Calculation of the proportion of spectra classified within each cluster for every voxel and participant (z-scored across voxels). By averaging the obtained z-values across subjects, we identified the brain generators of each spectral pattern. (E) Identification of natural frequencies, defined as the peak frequency of the centroid power spectrum with the largest z-value. (F) Computation of the median and 95% confidence interval for each voxel's natural frequency by means of bootstrapping.

2.5. Cluster analysis of power spectra

We applied k-means cluster analysis to identify different patterns of source-reconstructed oscillatory activity. To lighten computational load, 150 spectra per participant were randomly selected. Then, we concatenated the power spectra of every individual (128), voxel (1925), and time segment (150) and performed k-means clustering. The cosine was employed as the distance metric to maximise differences between clusters based on the shape of the spectra (Keitel & Gross, 2016). To optimise the results, we run 5 clustering replicates with a maximum number of 200 iterations each and accepted the one with the lowest sum of distances.

A key choice in k-means clustering is the number of clusters into which the data can be grouped. To select this parameter, we employed a cross-validation procedure for different initial numbers of clusters (5, 10, 15, 20, 25, 30, 40, 50, 75, 100, and 150). Due to the large amount of data to be clustered, conventional k-fold cross-validation techniques, such as k-fold cross-validation, would have required extremely long computation times. Hence, we adapted the approach to reduce computation time while taking advantage of the large amount of observations (>36 million). For each initial number of clusters, we randomly split our data into two halves. One half was employed to train the k-means algorithm. The second half was further subdivided into 100 test datasets. The data from each test dataset were then assigned to the clusters obtained from the training dataset. The average sum of distances to the centroids was used as a measure of accuracy, with smaller distances indicating a better fit. To check the consistency of the results, we repeated this procedure 5 times. As expected, the average sum of distances decreased as the number of clusters increased, with a very high degree of overlap for the 5 repetitions. Critically, the rate of improvement reached a plateau at around 25 clusters (see Supplementary Fig. 1A) and, therefore, this was the number of clusters selected. We thus detected 25 different spectral patterns, most of which were characterised by a peak at a single frequency (Fig. 1C).

As a further control, we repeated the whole analysis pipeline for different initial selections (5, 15, 25, 50, and 100 clusters) to double-check the consistency of our results for different clustering settings.

2.6. Brain regions underlying spectral patterns

The next step was to identify which brain regions were generating each spectral profile. For each subject and voxel, we calculated how many spectra — out of a maximum of 150 — were grouped within each cluster. The number of spectra belonging to each cluster was z-scored across voxels (i.e., for each voxel we subtracted the mean and divided by the standard deviation across voxels). This helped to minimise the impact of spatial leakage arising from dominant sources and frequency bands (e.g., parieto-occipital alpha). A larger z-value at a given voxel would thus indicate that oscillatory activity in this voxel is characterised by a specific spectral pattern or, in other words, that oscillations at a specific rate are more common in this voxel than in others.

The brain generators underlying each centroid power spectrum were identified by averaging the z-values obtained for each cluster and voxel across participants (Fig. 1D). Clusters reflecting gamma-band activity showed maximal z-values over the outer boundary of the cerebral cortex, surrounding the frontal, temporal, and occipital cortices. Since this result is most likely due to non-neural activity, such as microsaccades and/or electromyographic activity of facial and neck muscles (Muthukumaraswamy, 2013; Whitham et al., 2007), we only took into account clusters characterised by power spectra peaking below 30 Hz (i.e., 19 out of 25 clusters).

In addition, some clusters showed maximum z-values around the orbitofrontal cortex at slow frequencies (~2-3 Hz). To rule out the possibility that this activity could be a byproduct of remaining ocular artifacts,

we computed the pairwise correlation coefficient between each participant's z-value in the orbitofrontal voxel with the highest z-value and eye movements estimated from EOG recordings. Thus, we aimed to test whether or not individuals with more characteristic delta activity in the orbitofrontal region were also those with a greater amount of ocular activity. The amount of blinks and saccadic movements were estimated by calculating the standard deviation of the vertical EOG (VEOG) and horizontal EOG (HEOG) signals respectively. VEOG was available for all participants, although one of them was removed from the analysis for presenting high noise levels. HEOG was only available for 102 participants; two of them were also excluded due to noise.

A non-parametric permutation test was applied to evaluate which voxels were significantly associated with every spectral pattern. For each cluster, we conducted a one-sample t-test to compare each voxel's z-value with the mean z-value across voxels. We then estimated the distribution of test statistics under the null hypothesis by randomly shuffling (1000 times) z-values across voxels and computing t-tests against the mean z-value. In each iteration we stored the maximum t-statistic to correct for multiple comparisons. We then computed the 95th percentile of the permutation distribution. Voxels with z-values above this threshold were considered statistically significant.

2.7. Brain map of natural frequencies

Based on the above results, we created a brain map of natural frequencies. For each voxel and participant, we identified the spectral pattern with the highest z-value. The natural frequency of a given voxel was then defined as the peak frequency of the most characteristic power spectrum (Fig. 1E). In the event that an isolated voxel was equally associated with two spectral patterns, its natural frequency was interpolated by taking the mode of the neighbouring voxels. Although most spectra showed one single frequency peak, in a few cases the spectrum had more than one peak, usually a combination of alpha and beta-band activity (i.e., mu rhythm). In these cases, we weighted each frequency peak at 50%. Moreover, we tracked whether the natural frequency of each voxel came from a unimodal (e.g., single frequency peak in alpha/beta) or a bimodal (e.g., mu rhythm) spectrum.

We then employed a bootstrap approach to compute the natural frequency for each voxel across the whole sample along with the 95% confidence interval. First, participants were sampled with replacement 500 times. In each repetition, we computed the histogram of natural frequencies for each voxel. We then performed a Gaussian fit of all candidates' peak frequencies and selected the one with the highest goodness of fit. This step was computationally expensive but necessary, as simpler approaches such as computing the mean or the median across participants tend to provide solutions in the middle frequency range. The distribution of frequencies across bootstrap repetitions was used to derive the natural frequency (median) and the 95% confidence interval (2.5 and 97.5 percentiles) of each voxel (Fig. 1F).

We then tested whether the 95% confidence interval of each voxel was smaller than would be expected by chance. For this purpose, we repeated the above procedure 1000 times after randomly shuffling z-values across voxels. Thus, we estimated the distribution of the width of the confidence interval that one voxel would exhibit under random conditions. Width values below the 5th percentile of the permutation distribution were considered significantly smaller than expected by chance.

Additionally, we estimated the natural frequencies of the brain areas defined by the Automated Anatomical Labeling (AAL) atlas (Tzourio-Mazoyer et al., 2002). Although our analysis has been conducted on a single-voxel basis, identifying the typical frequency of commonly used regions of interest will enable comparison with previous studies. Thus, we detected the set of voxels located within each cortical and hippocampal region of the AAL template. Whilst the easiest approach would have then been to take the mean frequency across voxels, this was not the most appropriate strategy considering that the map of typical frequen-

cies contains several sharp transitions that do not overlap with the AAL parcellation (e.g., theta and high-beta oscillations in the superior frontal gyrus). To overcome this difficulty, we opted for detecting a representative voxel from each AAL region by performing k-means clustering on the natural frequencies of each set of voxels. The number of clusters was initially set to 4 to capture a large number of possible subdivisions within an AAL region. However, to obtain a more accurate result, we identified how many clusters were composed of a single voxel and repeated k-means clustering after removing them. We then detected which cluster contained a higher number of voxels and selected the voxel closer to the centroid as the most representative. The natural frequency and confidence interval of such voxel were then assigned to its corresponding AAL region.

2.8. Replicability analysis

We then evaluated whether the obtained distribution of natural frequencies was replicable by repeating the above procedure in two independent subsamples of participants. We randomly split the sample into two groups ($N=64$) and repeated the whole analysis pipeline for each sample separately. To quantify the replicability of our results we computed the correlation coefficient between the brain maps of natural frequencies obtained for each replicate sample.

2.9. Single-subject contributions

We also checked whether all participants contributed to some extent to all clusters or whether, on the contrary, some clusters were mainly driven by a subset of participants. This is important for the interpretation of the results, since it provides some clues about the primary source of spectral variability. In the first case, small variations in the peak frequency across clusters would be mainly accounted for by within-subject variability, whereas in the second case, they would be rather explained by between-subject variance.

2.10. Characterisation of spectral modes

In the preceding steps we developed a brain map of typical oscillatory activity during resting state. Thus, for every voxel in the brain we obtained a single value reflecting its natural frequency. However, ongoing oscillatory activity dynamically switches between different spectral modes (Keitel & Gross, 2016). Consequently, to provide a more comprehensive characterisation of the oscillatory profile of each brain region, we computed the median z-value for the representative voxel of each AAL region and for every canonical frequency band (delta, theta, alpha, mu, low-beta, high-beta).

Finally, we also identified the dominant frequencies of individual brain regions, i.e., the frequency that predominates most of the time in the recorded signal. For this purpose, we computed the percentage of time that oscillatory activity at every AAL brain region was clustered within each frequency band.

3. Results

3.1. Brain regions underlying spectral patterns

K-means clustering revealed 25 different spectral profiles, most of them characterised by a single peak in the power spectrum. By averaging the z-values of each cluster and voxel across participants, we identified the brain generators of each spectral pattern. As previously mentioned, we only considered clusters with peak frequencies below 30 Hz (i.e., 19 out of 25 clusters), since the generators of gamma-band oscillations were located outside the brain, surrounding frontal, temporal, and occipital regions (see Supplementary Fig. 2), which is suggestive of artifactual activity.

The generators of the remaining clusters are shown in Fig. 2. Only locations with z-values significantly different from zero are displayed ($p < .05$ corrected for multiple comparisons). As can be observed, our results show that each oscillatory frequency is generated by well-defined brain nodes. It is worth noting that although the analysis approach was purely data-driven, the frequencies associated with each brain node were naturally organized in a manner reminiscent of the canonical frequency bands: 1.5–4 Hz (delta), 4.5–7 Hz (theta), 8–13 Hz (alpha), and 14–30 Hz (beta). Not surprisingly, the dominant oscillatory frequency during the resting state was alpha. Six out of 19 clusters (31.6%) showed spectral peaks in the alpha band, in addition to two mu-rhythm clusters with peaks in both alpha and beta bands (10.5%).

Slow frequencies within the delta and theta range were generated by medial fronto-temporal cortical regions. In particular, we obtained three clusters with maximal z-values over the orbital part of the medial prefrontal cortex, as well as the left and right hippocampus. The corresponding power spectra peaked between 1.9 and 3.7 Hz, similar to the commonly established limits of the delta band. As a control, we tested the potential relationship between delta activity in the orbitofrontal cortex and ocular artifacts recorded by EOG. We did not find any significant correlation between delta activity and blinks ($R = .092$, $p = .302$) or between delta activity and saccades ($R = -.034$, $p = .741$), which suggests that orbitofrontal delta cannot be simply explained by remaining eye-movement artifacts. Moreover, three additional clusters showed spectra peaking in the theta range (4.7–7 Hz) and brain generators located around the medial superior frontal gyrus.

Interestingly, we identified two distinct varieties of alpha-band generators. First, we obtained three clusters with frequencies ranging between 9 and 11.6 Hz and a common prominent source located at the precuneus. Second, our results show a set of sources distributed bilaterally throughout sensory cortices, each of them characterised by a specific frequency peak: we found a generator peaking at 8.2 Hz over the auditory cortex, another source at 10.5 Hz around ventral visual areas, and finally a source at 12.8 Hz over dorsal visual areas.

In addition, we found two clusters with the characteristic spectrum of the mu-rhythm, i.e., a double peak in both the alpha and the beta-band (9.5/18.2 Hz and 11.6/22.2 Hz). Both sources were located over the somatomotor cortex, extending into parietal areas.

Finally, the brain sources of beta oscillations were distributed throughout lateral parietal and frontal regions, with increasing frequency following a posterior-to-anterior gradient. Specifically, low beta-band activity (14.9–17.3 Hz) was mostly generated by lateral occipitoparietal regions, whereas high beta-band oscillations were detected over motor (20.1 Hz) and prefrontal cortices (23.3–27.1 Hz).

3.2. Brain map of natural frequencies

The map of natural frequencies revealed a region-specific distribution of oscillatory activity characterised by both a medial-to-lateral and a posterior-to-anterior gradient of increasing frequency. As can be observed in Fig. 3A, medial frontal and temporal regions were characterised by lower rhythms (delta- and theta-band), posterior occipitotemporal cortices were dominated by alpha-band activity, while parietal areas mostly exhibited high-alpha and low-beta band activity. In contrast, motor and lateral prefrontal cortex were distinguished by high-beta activity.

The typical frequency of each voxel usually remained within a given frequency band as revealed by the 95% confidence interval maps (Fig. 3B). The confidence intervals were smaller than expected by chance in most voxels (98.3%). Only a small region in the orbital frontal gyrus showed a significantly larger confidence interval. This region lies at the confluence between the medial and lateral parts of the orbital frontal gyrus, which are characterised by extreme natural frequencies around 2 and 25 Hz respectively, thus explaining this result.

The perirolandic cortex also showed relatively wide confidence intervals. This region has a mixture of natural frequencies arising from both

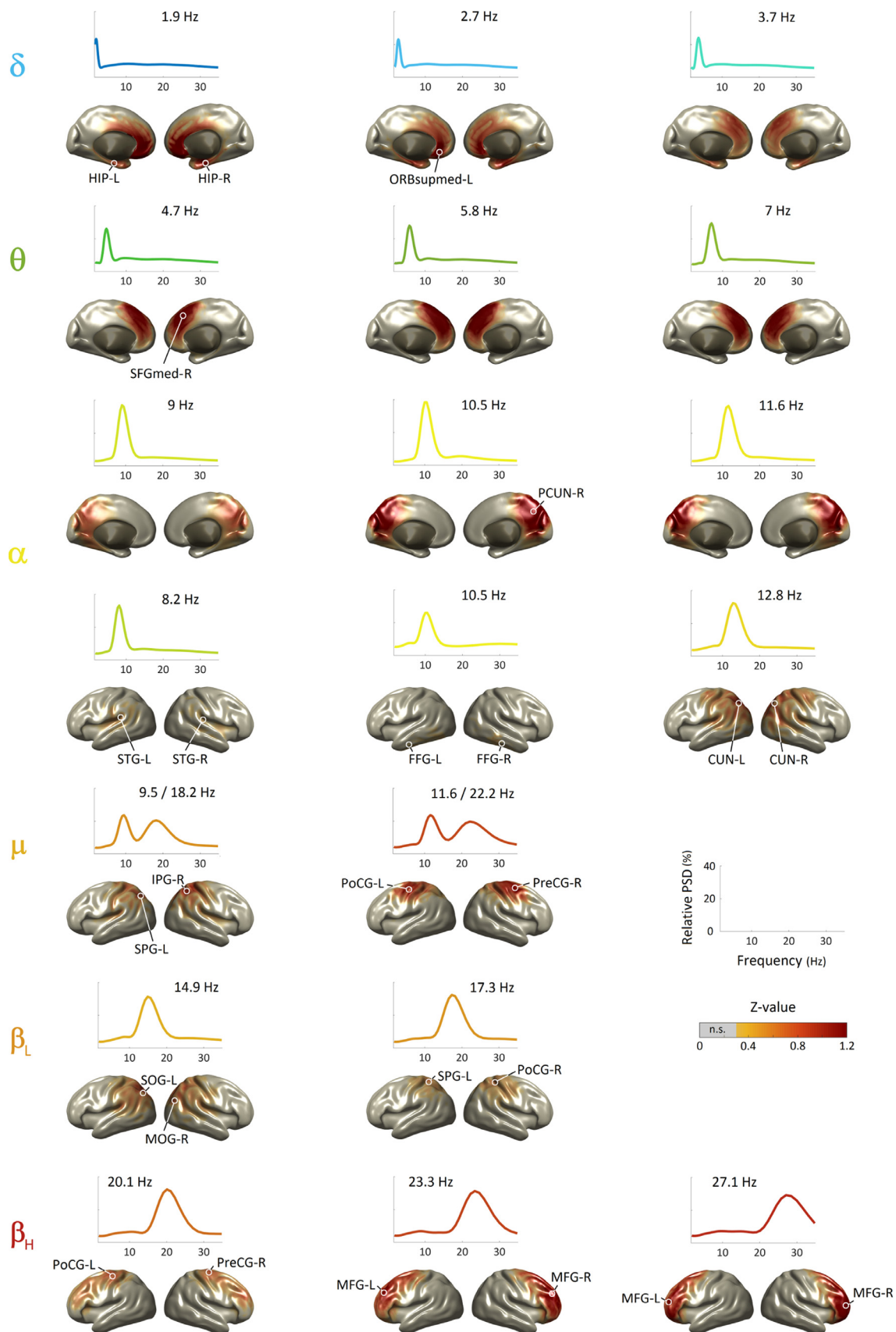


Fig. 2. Brain generators of centroid power spectra. The figure displays the brain sources underlying the oscillatory frequencies identified by k-means clustering. Slow frequencies (i.e., delta, theta) were generated by medial fronto-temporal regions. The brain sources of alpha oscillations were twofold: a generator located at the precuneus and a set of sources distributed throughout auditory and visual cortices. The mu-rhythm was originated from somatomotor regions. Beta sources were located throughout lateral parietal and frontal cortex, following a posterior-to-anterior gradient of increasing frequency. All brain maps have been thresholded at a p-level < .05 (corrected). White circles indicate local maxima. Abbreviations: L: left; R: right; HIP: hippocampus; ORBSupmed: superior frontal gyrus (medial orbital); SFGmed: superior frontal gyrus (medial); PCUN: precuneus; STG: superior temporal gyrus; FFG: fusiform gyrus; CUN: cuneus; SPG: superior parietal gyrus; IPG: inferior parietal gyrus; PoCG: postcentral gyrus; PreCG: precentral gyrus; SOG: superior occipital gyrus; MOG: middle occipital gyrus; MFG: middle frontal gyrus; PSD: power spectral density.

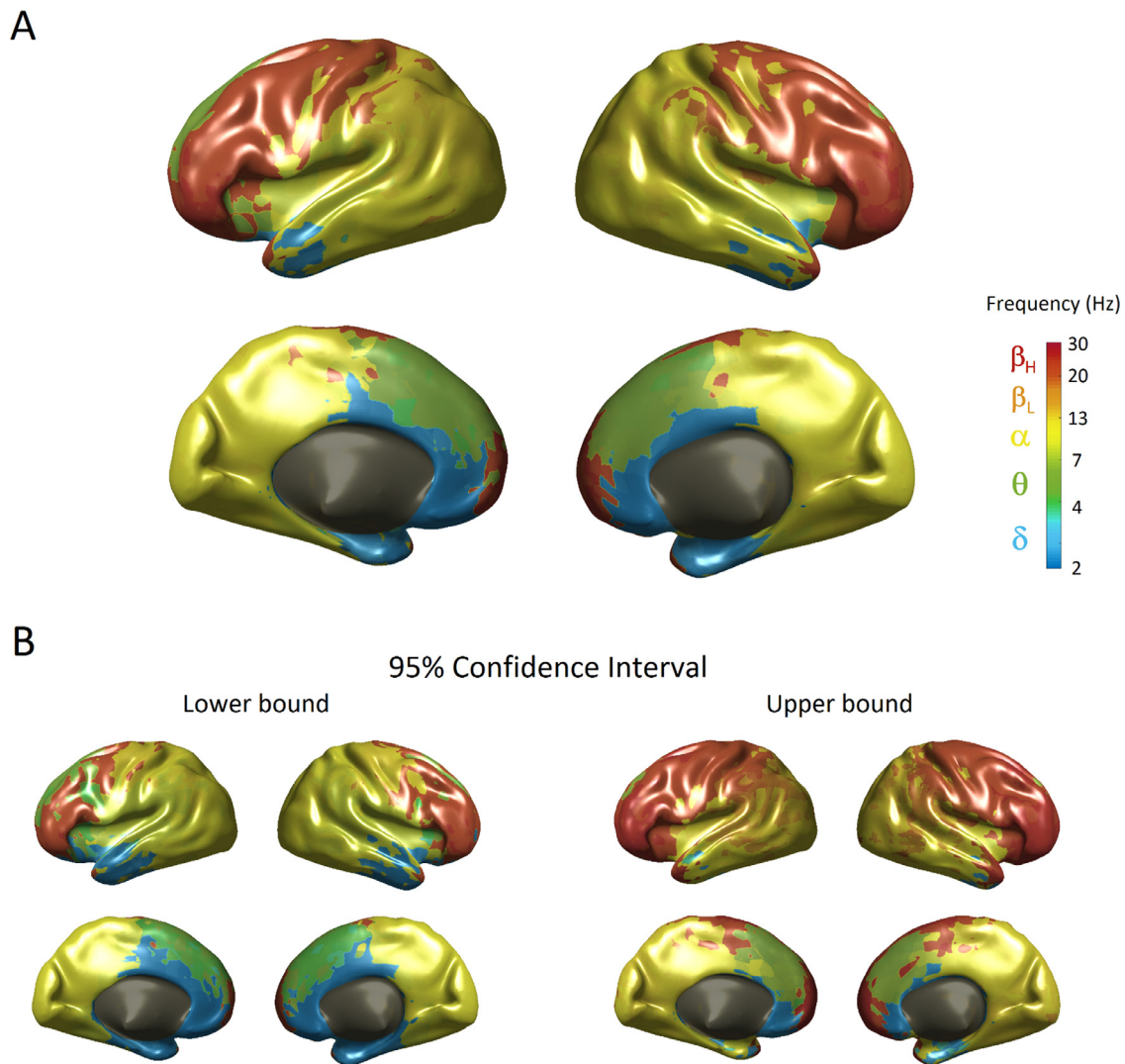


Fig. 3. Brain map of natural frequencies during resting. (A) Distribution of natural oscillations at the single-voxel level exhibiting both a medial-to-lateral and a posterior-to-anterior gradient of increasing frequency. Canonical frequency band ranges are color-coded to facilitate interpretation. (B) Lower and upper bounds of the 95% confidence interval estimated by a bootstrapping approach.

unimodal (alpha and beta) and bimodal (mu) power spectra. However, this feature was not taken into account in the previous analyses, as only one frequency per voxel was selected. Thus, to complement the brain map of natural frequencies, we carried out an additional analysis that examined whether the natural frequencies of each voxel came from unimodal or bimodal power spectra. As expected, our results showed that the majority of voxels with bimodal spectra were located around the somatomotor cortex (Fig. 4). However, the maximum number of participants showing natural frequencies from bimodal spectra was only 34.4%, indicating that unimodal spectra were predominant even in somatomotor regions.

In addition to the cortical surface representation, we have interpolated the results in a 3D volume in MNI space, creating an atlas that allows to look up the natural frequency, as well as the lower and upper bounds of the 95% confidence interval of specific MNI coordinates. The NIfTI files necessary to visualize the atlas can be found in the Supplementary Material. We have also created a Matlab function to easily retrieve the natural frequency and confidence interval at a given MNI coordinate (NaturalFreq.m, see Supplementary File 1).

Finally, the natural frequency and corresponding confidence interval for the cortical and hippocampal regions defined by the AAL atlas are listed in Table 1.

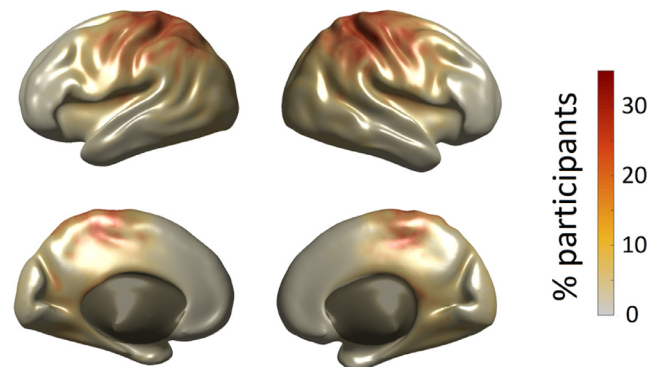


Fig. 4. Brain regions with natural frequencies arising from bimodal power spectra. Bimodal power spectra (i.e., mu rhythm) were typical of somatomotor regions, although they were only observed in a fraction of participants.

3.3. Control analyses: number of cycles and number of clusters

We conducted two additional control analyses to check that the parameters employed throughout the analysis procedure did not influence

Table 1

Natural frequency of AAL regions. Median natural frequency and 95% confidence interval of cortical and hippocampal AAL regions.

| AAL region | Natural Frequency | 95% Confidence Interval |
|-----------------------------------|-------------------|-------------------------|
| Precentral gyrus | 22.2 | [21.7, 22.7] |
| Superior frontal gyrus (dorsolat) | 23.1 | [22.7, 23.6] |
| Superior frontal gyrus (orb) | 23.4 | [22.8, 25.5] |
| Middle frontal gyrus | 23.5 | [23.1, 23.9] |
| Middle frontal gyrus (orb) | 25.3 | [23.6, 26.0] |
| Inferior frontal gyrus (oper) | 22.9 | [22.6, 23.4] |
| Inferior frontal gyrus (tri) | 23.2 | [22.8, 23.6] |
| Inferior frontal gyrus (orb) | 23.6 | [23.2, 25.5] |
| Rolandic operculum | 8.4 | [8.1, 9.8] |
| Supplementary motor area | 5.5 | [5.3, 5.6] |
| Olfactory cortex | 2.2 | [2.1, 2.4] |
| Superior frontal gyrus (med) | 5.6 | [5.5, 5.8] |
| Superior frontal gyrus (med orb) | 23.4 | [22.9, 25.5] |
| Rectus gyrus | 2.1 | [2.1, 2.2] |
| Insula | 22.6 | [5.5, 23.2] |
| Anterior cingulate gyrus | 5.5 | [4.6, 5.7] |
| Middle cingulate gyrus | 10.1 | [9.7, 11.4] |
| Posterior cingulate gyrus | 10.0 | [9.8, 10.3] |
| Hippocampus | 2.4 | [2.3, 2.5] |
| Parahippocampal gyrus | 2.3 | [2.1, 2.4] |
| Calcarine cortex | 11.8 | [10.4, 12.1] |
| Cuneus | 10.5 | [10.3, 11.7] |
| Lingual gyrus | 10.3 | [10.1, 10.5] |
| Superior occipital gyrus | 10.3 | [10.1, 10.6] |
| Middle occipital gyrus | 10.4 | [10.1, 11.8] |
| Inferior occipital gyrus | 10.5 | [10.3, 10.7] |
| Fusiform gyrus | 10.1 | [8.8, 11.5] |
| Postcentral gyrus | 21.4 | [19.2, 22.0] |
| Superior parietal gyrus | 11.5 | [10.4, 11.8] |
| Inferior parietal gyrus | 12.0 | [11.7, 12.4] |
| Supramarginal gyrus | 11.7 | [8.4, 12.2] |
| Angular gyrus | 12.1 | [11.7, 12.3] |
| Precuneus | 10.4 | [10.2, 11.4] |
| Paracentral lobule | 11.8 | [11.5, 12.1] |
| Heschl gyrus | 10.1 | [8.7, 11.8] |
| Superior temporal gyrus | 9.8 | [8.6, 10.2] |
| Temporal pole (sup) | 23.2 | [22.7, 23.7] |
| Middle temporal gyrus | 10.1 | [9.9, 10.4] |
| Temporal pole (middle) | 23.3 | [22.8, 23.8] |
| Inferior temporal gyrus | 10.1 | [9.9, 10.3] |

the results. In particular, we computed the brain map of natural frequencies for (i) frequency analyses performed with 3, 5, and 7 cycles per time window and (ii) different initial selections of the number of clusters (5, 15, 25, 50, and 100 clusters). As shown in Supplementary Fig. 1, our results indicate that the procedure for estimating natural frequencies is highly robust to variations in the analysis settings. The only parameter that substantially affected the results was the selection of only 5 clusters, as it failed to identify any clusters in the delta range.

3.4. Replicability analysis

The correlation coefficient between the brain maps of natural frequencies derived from two independent subsamples ($N = 64$) was 0.787 ($p < .001$), indicating that the replicability of our results is considerably high (see Fig. 5).

3.5. Single-subject contributions

The single-subject natural frequency brain maps obtained from the first 30 individuals in the sample are displayed in Supplementary Fig. 3. Each participant is identified by its corresponding subject ID from the OMEGA database. Despite some expected variability, both the medial-to-lateral and the posterior-to-anterior gradients of increasing frequency can be observed to some extent at the single-subject level. It is important to mention that the single-subject natural frequencies have been estimated from only 150 power spectra per participant, as the use of

a larger volume of data was too computationally expensive. However, more accurate frequency maps could be obtained at the single-subject level by assigning a larger number of power spectra from a single participant to the clusters previously obtained from the whole sample.

We also tested how much each participant contributed to each cluster. In the ideal case where the contribution of all participants is perfectly balanced, the expected weight of each participant in each cluster would be 0.781% (i.e., $100/128$). We found that the minimum contribution of an individual to a cluster was 0.203 ± 0.096 % and the maximum contribution was 2.006 ± 0.399 %. It is important to note that all clusters comprised data from 100% of participants, indicating that clustering was not driven by a subset of individuals. Overall, these results suggest that peak frequency shifts between similar clusters reflect within- rather than between-subject variability.

3.6. Characterisation of spectral modes

Finally, we computed the weights of different spectral modes to further characterise the oscillatory profile of each brain area beyond its natural frequency. As can be observed in Fig. 6A, most AAL regions showed more than one characteristic spectral mode. In some cases, these reflected contiguous frequency bands (e.g., delta and theta in the rectus gyrus, or alpha/mu/low-beta in the superior parietal gyrus). In other cases, different spectral modes might reflect the natural frequencies of several functional sub-parcellations of one single region (e.g., theta and high-beta along the superior frontal gyrus), as the anatomical bound-

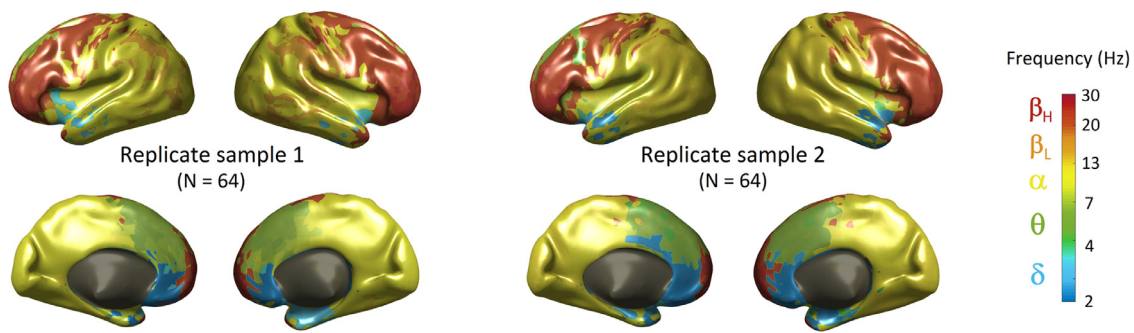


Fig. 5. Replicability of the brain map of natural frequencies. The figure shows the brain maps estimated from two independent subsamples.

aries of the AAL atlas did not completely fit with the transitions between natural frequencies. It is also worth noting that some regions, particularly throughout the temporal lobe (e.g., middle and inferior temporal gyrus), did not exhibit typical oscillatory frequencies at any of the canonical frequency bands.

To complement the characterisation of ongoing oscillatory activity, we additionally identified the dominant frequencies of each AAL brain region by computing the percentage of time spent in each spectral mode (Fig. 6B). Contrasting with the heterogeneity observed for natural frequencies (Fig. 6A), brain activity was mostly dominated by a single mode in the alpha frequency range, especially in the posterior cortex. Dominant frequencies in frontal areas were found to be more evenly distributed among theta, alpha and beta bands.

4. Discussion

This study presents the most comprehensive map of the typical oscillatory activity of the resting human brain performed to date. We applied a fully data-driven procedure to identify precise natural frequencies at a single-voxel level. Our results reveal a region-specific organisation of ongoing oscillations defined by both a medial-to-lateral and a posterior-to-anterior gradient of increasing frequency. In particular, medial fronto-temporal areas were characterised by slow (delta/theta) rhythms. Posterior regions exhibited natural frequencies within the alpha band, with specific generators in the precuneus, visual, and auditory sensory cortices. Mu activity was characteristic of somatomotor regions, while the lateral prefrontal cortex was distinguished by oscillations in the high beta range. Critically, our results provided empirical validation of the classical frequency bands and were highly reproducible in two independent subsamples of individuals.

In the following paragraphs, we will first discuss the critical methodological features of the present study in comparison with prior work. We will then address the distinction between the concepts of natural frequency and dominant frequency. Subsequently, we will examine the results obtained for each frequency band. Whereas some results corroborate well established knowledge, such as the neural underpinnings of alpha and theta rhythms, others provide novel information on frequency bands on which there is less consensus, such as delta or beta. Finally, we will discuss the potential relationship between natural frequencies and resting state networks (RSNs).

4.1. Methodological remarks

The present study combined a series of methodological innovations that, taken together, significantly contribute to the characterisation of intrinsic brain oscillations. First, analyses were performed on MEG data obtained from a very large ($N=128$) and representative (age range 19–73 years) sample of healthy adult volunteers. The recently developed iEEG atlas of electrophysiological brain activity has also been created from a large database, in this case recorded from patients with epilepsy

(Frauscher et al., 2018; Kalamangalam et al., 2020). However, the ethical constraints associated with electrode placement make it more difficult to systematically map oscillatory activity throughout the brain by means of iEEG.

Second, according to our data-driven strategy, and in contrast to previous work (Keitel & Gross, 2016; Mahjoory et al., 2020), we did not parcellate the brain into predefined regions of interest based on anatomical criteria. Our results reveal that the brain displays similar rhythmic patterns in neighbouring voxels, which could be grouped into functionally equivalent areas. Importantly, the anatomical and functional parcellations do not completely overlap, as some abrupt transitions in natural frequencies do not have an anatomical correspondence. Future research could extend the current results to elaborate a functional parcellation based on the brain's intrinsic oscillatory dynamics, similar to the functional organisation of the brain derived from fMRI resting state connectivity analysis over the last decade (Eickhoff et al., 2018; Yeo et al., 2011).

Finally, unlike most previous work, we did not employ predetermined frequency bands. Instead, we identified exact frequency peaks in power spectrum centroids obtained from k-means clustering. Critically, spectral peak detection has recently been emphasized as a requisite to verify the presence of true oscillatory activity (Donoghue et al., 2021). Nevertheless, despite not having defined frequency bands *a priori*, they emerged empirically from the data. Based on their underlying brain generators, centroid power spectra could be organised into the following frequency ranges: 1.5–4 Hz for delta, 4.5–7 Hz for theta, 8–13 Hz for alpha, and 14–30 Hz for beta. These fit well with the standard classification of brain rhythms as well as with the empirical definition of frequency bands obtained with other methodological approaches (Mahjoory et al., 2020). Noteworthy, while having been used for decades, canonical frequency bands have a striking lack of empirical support. Our results represent a pioneering effort in this direction and could be extended in the future by identifying more fine-grained frequency boundaries. The gedBounds approach recently developed by Cohen (2021) could be particularly well suited for this purpose.

4.2. Natural frequencies Vs. Dominant frequencies

A fundamental distinction must be made between the concepts of dominant and natural frequency. On the one hand, dominant frequency could be defined as the most prevalent oscillatory rhythm of a brain region, i.e., the frequency that predominates most of the time. On the other hand, natural frequency would refer to the spectral pattern that characterises an individual brain area or, in other words, the oscillatory frequency that is most often observed in a given region in comparison with other parts of the brain. As our results show, dominant and natural frequencies do not necessarily coincide (see Fig. 5). An example is the tau rhythm (~8.5 Hz) which albeit not dominant, is the characteristic local rhythm of the auditory cortex as corroborated by its reactivity to sounds in previous research (Lehtelä et al., 1997; Tiitonen et al., 1991).

| | A | | | | | | B | | | | | |
|-----------------------------------|---------------------|----------|----------|-------|-----------|-----------|----------------------|----------|----------|-------|-----------|-----------|
| | Natural frequencies | | | | | | Dominant frequencies | | | | | |
| | δ | θ | α | μ | β_L | β_H | δ | θ | α | μ | β_L | β_H |
| Precentral gyrus | -0.5 | -0.0 | 0.2 | 0.7 | 0.3 | 0.5 | 6.3 | 11.8 | 32.4 | 10.1 | 10.8 | 18.1 |
| Superior frontal gyrus (dorsolat) | 0.4 | 0.7 | -0.6 | -0.3 | -0.2 | 1.3 | 10.7 | 17.0 | 16.1 | 5.8 | 8.0 | 21.6 |
| Superior frontal gyrus (orb) | 0.1 | 0.4 | -0.8 | -0.5 | -0.2 | 0.8 | 10.2 | 14.2 | 13.5 | 4.8 | 7.4 | 17.9 |
| Middle frontal gyrus | -0.3 | 0.1 | -0.7 | -0.4 | -0.2 | 1.1 | 7.3 | 12.7 | 16.5 | 5.7 | 7.9 | 20.5 |
| Middle frontal gyrus (orb) | 0.0 | -0.1 | -0.8 | -0.5 | -0.3 | 1.0 | 9.2 | 11.3 | 13.7 | 5.0 | 7.2 | 19.7 |
| Inferior frontal gyrus (oper) | -0.1 | 0.3 | -0.3 | 0.1 | -0.1 | 0.7 | 8.3 | 14.3 | 22.5 | 7.6 | 8.6 | 19.3 |
| Inferior frontal gyrus (tri) | -0.3 | 0.1 | -0.8 | -0.4 | -0.3 | 1.1 | 7.7 | 12.5 | 15.1 | 5.3 | 7.7 | 20.6 |
| Inferior frontal gyrus (orb) | -0.2 | -0.3 | -0.8 | -0.5 | -0.4 | 0.7 | 7.7 | 9.7 | 14.3 | 5.0 | 6.6 | 17.9 |
| Rolandic operculum | 0.1 | 0.3 | 0.5 | 0.5 | 0.2 | -0.3 | 10.3 | 14.2 | 37.0 | 9.2 | 10.6 | 10.7 |
| Supplementary motor area | 0.1 | 1.2 | -0.7 | -0.5 | -0.5 | 0.7 | 10.2 | 20.7 | 17.0 | 5.1 | 6.4 | 18.4 |
| Olfactory cortex | 0.8 | 0.3 | -0.4 | -0.2 | -0.3 | 0.1 | 14.2 | 14.0 | 21.5 | 6.2 | 7.5 | 13.7 |
| Superior frontal gyrus (med) | 0.3 | 0.9 | -0.8 | -0.6 | -0.3 | 0.6 | 11.3 | 17.6 | 13.9 | 4.5 | 7.2 | 17.0 |
| Superior frontal gyrus (med orb) | -0.1 | 0.2 | -0.9 | -0.6 | -0.4 | 0.7 | 8.6 | 12.6 | 11.9 | 4.4 | 6.9 | 17.2 |
| Rectus gyrus | 0.8 | 0.4 | -0.6 | -0.3 | -0.2 | 0.4 | 14.2 | 14.8 | 18.1 | 5.9 | 8.1 | 16.1 |
| Insula | 0.6 | 0.9 | -0.4 | 0.0 | -0.0 | 0.9 | 13.4 | 17.9 | 20.5 | 7.2 | 8.7 | 19.6 |
| Anterior cingulate gyrus | 0.4 | 1.2 | -0.6 | -0.3 | -0.1 | 0.9 | 12.2 | 20.4 | 17.2 | 5.8 | 8.3 | 19.2 |
| Middle cingulate gyrus | 0.4 | -0.0 | 0.4 | 0.2 | -0.1 | -0.4 | 11.9 | 11.6 | 36.8 | 8.0 | 9.0 | 10.5 |
| Posterior cingulate gyrus | 0.3 | -0.2 | 0.7 | 0.2 | 0.1 | -0.7 | 10.9 | 10.2 | 44.2 | 8.1 | 10.3 | 7.9 |
| Hippocampus | 0.4 | 0.1 | 0.5 | 0.2 | 0.2 | -0.6 | 11.8 | 12.5 | 37.9 | 7.8 | 10.4 | 8.7 |
| Parahippocampal gyrus | 0.7 | 0.1 | -0.3 | -0.4 | -0.5 | -0.4 | 13.2 | 12.1 | 23.7 | 5.7 | 6.8 | 10.1 |
| Calcarine cortex | -0.4 | -0.7 | -0.0 | -0.5 | -0.3 | -0.7 | 6.0 | 6.4 | 29.7 | 5.3 | 8.5 | 7.5 |
| Cuneus | -0.1 | -0.4 | 0.9 | 0.4 | 0.4 | -0.8 | 8.4 | 9.2 | 47.9 | 8.5 | 11.8 | 7.7 |
| Lingual gyrus | -0.9 | -1.0 | -0.3 | -0.5 | -0.4 | -0.6 | 3.2 | 4.5 | 25.1 | 4.9 | 7.3 | 8.6 |
| Superior occipital gyrus | -0.1 | -0.4 | 0.9 | 0.3 | 0.3 | -0.8 | 7.6 | 8.8 | 48.1 | 8.3 | 11.3 | 6.9 |
| Middle occipital gyrus | -0.1 | -0.2 | 0.7 | 0.2 | 0.4 | -0.7 | 8.1 | 9.9 | 41.0 | 7.8 | 11.6 | 7.8 |
| Inferior occipital gyrus | -0.6 | -0.8 | 0.1 | -0.2 | -0.1 | -0.5 | 4.6 | 6.1 | 30.3 | 6.2 | 9.1 | 8.5 |
| Fusiform gyrus | 0.9 | 0.3 | 0.0 | -0.3 | -0.3 | -0.5 | 15.5 | 14.1 | 28.1 | 6.0 | 7.9 | 9.4 |
| Postcentral gyrus | -0.5 | -0.2 | 0.3 | 0.7 | 0.5 | 0.3 | 5.8 | 10.2 | 33.8 | 9.9 | 12.0 | 15.9 |
| Superior parietal gyrus | -0.7 | -0.6 | 0.6 | 0.5 | 0.4 | -0.3 | 5.1 | 7.6 | 41.1 | 9.2 | 11.5 | 11.0 |
| Inferior parietal gyrus | -0.3 | -0.2 | 0.6 | 0.6 | 0.7 | -0.2 | 7.1 | 10.6 | 40.0 | 9.4 | 13.0 | 11.7 |
| Supramarginal gyrus | -0.1 | 0.0 | 0.6 | 0.7 | 0.5 | -0.2 | 8.8 | 12.1 | 37.5 | 9.8 | 12.3 | 11.6 |
| Angular gyrus | -0.3 | -0.4 | 0.6 | 0.2 | 0.4 | -0.7 | 6.8 | 8.8 | 41.9 | 7.9 | 11.7 | 8.3 |
| Precuneus | -0.4 | -0.4 | 0.8 | 0.5 | 0.4 | -0.5 | 7.0 | 9.0 | 44.8 | 8.9 | 11.3 | 9.6 |
| Paracentral lobule | -0.3 | -0.1 | 0.3 | 0.6 | 0.1 | 0.1 | 7.5 | 10.9 | 37.2 | 9.3 | 9.8 | 13.8 |
| Heschl gyrus | 0.0 | -0.2 | 0.1 | 0.1 | 0.2 | -0.2 | 9.4 | 10.3 | 30.5 | 7.4 | 10.4 | 10.9 |
| Superior temporal gyrus | 0.2 | -0.2 | 0.0 | -0.3 | -0.2 | -0.5 | 10.7 | 10.7 | 28.7 | 5.8 | 8.4 | 9.1 |
| Temporal pole (sup) | 0.0 | -0.1 | -0.7 | -0.5 | -0.4 | 0.4 | 9.2 | 11.0 | 15.7 | 5.1 | 7.1 | 15.5 |
| Middle temporal gyrus | -0.4 | -0.5 | -0.1 | -0.5 | -0.0 | -0.5 | 6.5 | 8.2 | 27.9 | 5.3 | 9.3 | 8.7 |
| Temporal pole (middle) | 0.6 | -0.0 | -0.3 | -0.5 | -0.4 | -0.2 | 13.1 | 12.0 | 22.3 | 5.1 | 7.1 | 10.4 |
| Inferior temporal gyrus | -0.3 | -0.5 | -0.2 | -0.4 | -0.3 | -0.6 | 7.4 | 8.3 | 25.2 | 5.7 | 8.1 | 8.1 |

Fig. 6. Spectral modes for natural and dominant frequencies at different AAL brain regions. (A) Natural frequencies were indexed by z-values (i.e., how typical is activity in a given frequency band at a specific region compared with other regions). Note that most AAL brain areas were engaged in several characteristic spectral modes. (B) Dominant frequencies were computed as the percentage of time spent in each spectral mode (i.e., how predominant is activity in a given frequency band). The figure shows the high predominance of alpha-band activity, particularly in posterior regions.

At a methodological level, the common approach of averaging power spectra tends to emphasise dominant frequencies (Hillebrand et al., 2012; Mahjoory et al., 2020; Mellem et al., 2017; Niso et al., 2016; Niso et al., 2019). In contrast, clustering-based techniques allow the identification of non-dominant patterns present on single trials, thus enabling the identification of natural frequencies (Frauscher et al., 2018; Keitel & Gross, 2016). However, a common problem is that a highly dominant source, such as the posterior alpha rhythm, may obscure oscillatory activity in neighbouring regions. In this study, we applied z-score normalisation to mitigate the potential confounding effect of source leakage.

To date, the concept of natural frequency has almost exclusively been employed to refer to the main frequency evoked by direct electrical/magnetic stimulation of a given brain region (Amengual et al., 2019; Ferrarelli et al., 2012; Rosanova et al., 2009). In this study, we have developed a map of natural frequencies that is highly compatible with the results obtained by direct cortical perturbation, but without interfering with ongoing brain activity. It is worth noting that an advantage of our approach is that it allows the extraction of whole-brain natural frequencies with a wide and homogeneous spatial coverage from 5-minute resting state recordings.

4.3. Brain generators underlying canonical frequency bands

Unsurprisingly, our first finding was that the alpha rhythm is clearly dominant in the brain: most clusters were characterised by an alpha peak (Fig. 2) and for most of the time rhythmic brain activity oscillated around 10 Hz in the majority of brain regions, with the exception of frontal areas (Fig. 6B). A first type of alpha generator, peaking at around 10.5 Hz, was located in the precuneus, in agreement with pioneering work that identified this brain area as the main source of posterior alpha activity (Hari et al., 1997; Salmelin & Hari, 1994). Further, the precuneus/posterior cingulate cortex (PCC) is considered a key hub of the default mode network (DMN) (Fransson & Marrelec, 2008; Raichle et al., 2001) and, therefore, this generator could be referred to as 'default-alpha'. A second type of alpha-band generators was distributed over visual, auditory, and somatosensory (linked to mu-rhythm) cortices, in agreement with prior evidence (Haegens et al., 2015; Hari & Salmelin, 1997; Salmelin & Hari, 1994). Each sensory-specific alpha was characterised by a particular cortical distribution and natural frequency, such as the 'visual-alpha' with frequencies in the upper alpha range (10.5–13 Hz) (Barzegaran et al., 2017; Hindriks et al., 2017) or the 'auditory-alpha' (i.e., 'tau' rhythm) with a lower natural frequency at around 8.5 Hz (Lehtelä et al., 1997; Tiihonen et al., 1991).

We found somatosensory alpha linked to the mu rhythm over perirolandic cortex. Mu oscillations are characterised by a comb-shaped waveform and a spectrum with a double peak in the alpha and beta bands (Tiihonen et al., 1989). The prevailing view is that the mu rhythm arises from the superposition of an alpha component originating in the somatosensory cortex and a beta component reflecting activity from the precentral motor cortex (Hari & Salmelin, 1997), which would be mixed due to source proximity and volume conduction. Our results support this notion, since we observed a predominance of postcentral alpha and precentral beta (Fig. 3), coming in ~35% of cases from bimodal spectra (mu rhythm) (Fig. 4). However, it is important to note that our analyses were based solely on the shape of power spectra. It would be important to test whether the non-sinusoidal mu waveform, in which one part of the wave (e.g., trough) is consistently sharper than the other (e.g., peak) (Cole & Voytek, 2017), can be explained by the superposition of ~10 Hz and ~20 Hz oscillations. Therefore, future research using a waveform-based analysis approach would be necessary to disentangle whether the mu rhythm actually exists or is simply a combination of somatosensory-alpha and motor-beta oscillations (Cole & Voytek, 2019).

Theta oscillations are often observed at the scalp level with a characteristic topographical distribution, centred over midline fronto-

central sites (Scheeringa et al., 2008). Brain sources underlying mid-frontal theta have been consistently located near dorsal anterior cingulate cortex (ACC) or medial prefrontal cortex (Gevins et al., 1997; Onton et al., 2005). This is highly consistent with the brain regions showing natural frequencies within the theta range found here, as well as with the location of the resting state theta-band generators reported by previous studies (Kalamangalam et al., 2020; Mellem et al., 2017; Niso et al., 2016). Moreover, midfrontal theta oscillations are commonly induced by highly demanding cognitive tasks, such as mental arithmetic, error detection, response conflict, or working memory tasks (Gartner et al., 2015; Gevins et al., 1997; Zuure et al., 2020). Taking into consideration both anatomical and functional evidence, it might be suggested that theta oscillations arising from medial prefrontal cortex underlie the RSN of executive control and working memory previously identified with fMRI (Cavanagh & Frank, 2014; Damoiseaux et al., 2006).

The two brain areas characterised by natural frequencies in the delta band were the medial orbitofrontal cortex and the hippocampal region. The orbitofrontal cortex has been pointed out as generator of slow oscillations at rest (Congedo et al., 2010; Hillebrand et al., 2012; Niso et al., 2016; Niso et al., 2019) and during sleep, in which they propagate as travelling waves towards posterior regions periodically modifying the state of cortical excitability and connectivity (Massimini et al., 2004). The hippocampus and parahippocampal gyrus showed natural frequencies in the delta range, around 2–3 Hz. This finding is consistent with the iEEG atlas developed by Frauscher and colleagues (2018), although it seems at first to contradict the common notion that theta oscillations underlie hippocampal function (Herweg et al., 2020). However, this apparent contradiction might be overcome by evidence that theta oscillations become slower with increasing brain size (Buzsáki et al., 2013). Thus, rodent theta oscillations (~4–10 Hz) might be expressed in humans at lower frequencies, within the delta band (~1–4 Hz) (Jacobs, 2014). It could also be possible that both delta and theta-band oscillations coexist in different parts of the hippocampus. In fact, we found a sharp transition between the natural frequencies of the anterior (~2–2.5 Hz) and the posterior (~8–8.5 Hz) portion of the hippocampus. Since the anterior and posterior hippocampus are known to be functionally distinct (Fanselow and Dong, 2010; Zeidman, 2016), an intriguing possibility is that this dissociation is expressed in specific oscillatory dynamics. In support of this idea, some studies have identified two different types of hippocampal oscillations at 2–3 Hz and ~8 Hz during memory processes (Lega et al., 2012; Watrous et al., 2013). However, given the limited spatial resolution of MEG, further investigation with iEEG would be necessary to confirm this finding.

Finally, beta oscillations have traditionally been considered a signature of the resting motor cortex (Jasper & Penfield, 1949). Most previous research supports this view, showing that beta activity mainly arises from perirolandic regions (Frauscher et al., 2018; Hillebrand et al., 2012; Niso et al., 2016). Only a few previous studies have also pointed to beta as the characteristic rhythm of the prefrontal cortex (Mahjoory et al., 2020; Mellem et al., 2017). Our results provide a more complete overall picture of the beta rhythm, by showing that perirolandic and lateral prefrontal regions are distinguished by oscillations in the lower and upper beta range, respectively. Furthermore, we found that oscillatory activity in the lateral prefrontal cortex is not homogeneous but rather characterised by a posterior-to-anterior gradient of increasing frequency, in agreement with prior reports (Ferrarelli et al., 2012; Mahjoory et al., 2020). Intriguingly, this gradient is reminiscent of Koechlin's theory of cognitive control, which considers that the lateral prefrontal cortex is functionally organised as a cascade of executive processes that are hierarchically ordered along the anterior-posterior axis (Koechlin & Summerfield, 2007). Therefore, it might be speculated that a progressively increasing frequency within the beta band indexes the multistage functional architecture of the lateral prefrontal cortex.

4.4. Natural frequencies and resting state networks (RSNs)

Given the pivotal role of brain oscillations in brain communication (Buzsáki & Watson, 2012; Fries, 2015; Varela et al., 2001), an arising question is whether natural frequencies are somehow related to network connectivity. At first, one might expect different nodes of the same RSN to share the same natural frequency in order to facilitate synchronisation. However, our results do not support this idea. For example, the main nodes of the DMN are characterised by natural frequencies in virtually all frequency bands. Nonetheless, a mismatch in natural frequencies does not preclude network communication, since this can be attained through different mechanisms involving cross-frequency amplitude, phase, or phase-amplitude coupling (Palva & Palva, 2018; Roupun et al., 2008; Siegel et al., 2012).

An interesting possibility is that brain regions might transiently abandon their natural frequencies, adopting a different spectral mode to synchronise at the same frequency. This would be in line with the recent view that RSNs are non-stationary, but rather characterised by short-lived transient brain states (Vidaurre et al., 2018). During these microstates, different parts of the network may synchronise at a particular frequency. For instance, it has been found that the anterior and posterior portions of the DMN synchronise at the typical frequency of the anterior region, i.e., in the delta/theta range (1–7 Hz) (Vidaurre et al., 2018). Thus, the PCC might briefly leave its natural frequency in the alpha range to communicate with the anterior DMN in a slower frequency channel. Our results are compatible with this scenario, since all brain regions show activity in several spectral modes beyond their natural frequency (Fig. 6A; see also Keitel & Gross, 2016), which is suggestive of a dynamically changing state of the oscillatory brain activity.

5. Conclusions

Here we have presented the first MEG-based atlas of the natural frequencies of the human brain at rest. Overall, our results show that the brain exhibits a characteristic and highly replicable pattern of ongoing oscillatory activity, which is organised according to both an anterior-posterior and a medial-lateral axis. We believe that these findings will contribute to further elucidate the functional architecture of the human brain.

Data and code availability statement

Data were obtained from the Open MEG Archive (OMEGA) (<https://www.mcgill.ca/bic/resources/omega>). All scripts necessary to reproduce the analysis and the figures in this paper are available at <https://github.com/necog-UAM/OMEGA-NaturalFrequencies>.

Author Contributions

Almudena Capilla: Conceptualization, Data curation, Formal analysis, Funding acquisition, Methodology, Software, Visualization, Writing – original draft preparation; **Lydia Arana:** Validation, Writing – original draft preparation; **Marta García-Huésca:** Formal analysis, Writing – review & editing; **María Melcón:** Resources, Writing – review & editing; **Joachim Gross:** Conceptualization, Writing – review & editing; **Pablo Campo:** Conceptualization, Funding acquisition, Writing – review & editing

Declaration of Competing Interest

The authors declare no competing interests.

Acknowledgements

We are thankful to the team of researchers and technicians involved in The Open MEG Archive (OMEGA) project for recording and making publicly available the database employed in the present study and,

particularly, to Guiomar Niso for introducing us to this initiative. The authors also thank Abel Cano, Enrique Stern, and Dominique Kessel for valuable methodological advice.

This work was supported by FEDER/Ministerio de Ciencia, Innovación y Universidades – Agencia Estatal de Investigación, Spain (grant PGC2018-100682-B-I00 to AC and PC) and the Comunidad de Madrid POEJ/FSE (grant PEJD-2017-PRE/SOC-3859 to AC). MM was supported by the Universidad Autónoma de Madrid (FPI-UAM-2017 fellowship). JG was supported by Deutsche Forschungsgemeinschaft (GR 2024/5-1 and GR 2024/8-1). The funders had no role in study design, data collection and analysis, decision to publish, or preparation of the manuscript.

Supplementary materials

Supplementary material associated with this article can be found, in the online version, at doi:10.1016/j.neuroimage.2022.119373.

References

- Amengual, J.L., Stengel, C., Moreau, T., Adam, C., Chavez, M., Valero-Cabré, A., 2019. Perturbation-based mapping of natural frequencies with direct intracranial stimulation of the human brain. *BioRxiv* doi:10.1101/718064.
- Basar, E., et al., 1992. Brain natural frequencies are causal factors for resonances and induced rhythms. In: Baar, E., et al. (Eds.), *Induced Rhythms in the Brain*. Springer, pp. 425–467 Science+Business Media.
- Barzegaran, E., Vildavski, V.Y., Knyazeva, M.G., 2017. Fine Structure of Posterior Alpha Rhythm in Human EEG: Frequency Components, Their Cortical Sources, and Temporal Behavior. *Sci. Rep.* 7 (1), 1–12. doi:10.1038/s41598-017-08421-z.
- Besl, P.J., McKay, N.D., 1992. A Method for Registration of 3-D Shapes. *IEEE Trans. Pattern Anal. Mach. Intell.* 14 (2), 239–256. doi:10.1109/34.121791.
- Boersma, M., Smit, D.J.A., De Bie, H.M.A., Van Baal, G.C.M., Boomsma, D.I., De Geus, E.J.C., Delemarre-Van De Waal, H.A., Stam, C.J., 2011. Network analysis of resting state EEG in the developing young brain: Structure comes with maturation. *Hum. Brain Mapp.* 32 (3), 413–425. doi:10.1002/hbm.21030.
- Buzsáki, G., 2006. *Rhythms of the Brain*. Oxford University Press doi:10.1093/acprof:oso/9780195301069.001.0001.
- Buzsáki, G., Logothetis, N., Singer, W., 2013. Scaling brain size, keeping timing: Evolutionary preservation of brain rhythms. *Neuron* 80 (3), 751–764. doi:10.1016/j.neuron.2013.10.002.
- Buzsáki, G., Watson, B.O., 2012. Brain rhythms and neural syntax: Implications for efficient coding of cognitive content and neuropsychiatric disease. *Dialogues in Clinical Neuroscience* 14 (4), 345–367. doi:10.31887/dcms.2012.14.4/gbuzsaki.
- Cavanagh, Frank, M.J., 2014. Frontal Theta as a Mechanism for Affective and Effective Control. *Trends Cogn. Sci.* 18 (8), 414–421. doi:10.1016/j.tics.2014.04.012.Frontal.
- Chen, A.C.N., Feng, W., Zhao, H., Yin, Y., Wang, P., 2008. EEG default mode network in the human brain: Spectral regional field powers. *Neuroimage* 41 (2), 561–574. doi:10.1016/j.neuroimage.2007.12.064.
- Cohen, M.X., 2021. A data-driven method to identify frequency boundaries in multichannel electrophysiology data. *J. Neurosci. Methods* 347, 108949. doi:10.1016/j.jneumeth.2020.108949.
- Cole, S.R., Voytek, B., 2017. Brain oscillations and the importance of waveform shape. *Trends Cogn. Sci.* 21 (2), 137–149. doi:10.1016/j.tics.2016.12.008.
- Cole, S., Voytek, B., 2019. Cycle-by-cycle analysis of neural oscillations. *J. Neurophysiol.* 122 (2), 849–861. doi:10.1152/jn.00273.2019.
- Congedo, M., John, R.E., De Ridder, D., Pritchep, L., 2010. Group independent component analysis of resting state EEG in large normative samples. *Int. J. Psychophysiol.* 78 (2), 89–99. doi:10.1016/j.ijpsycho.2010.06.003.
- Damoiseaux, J.S., Rombouts, S.A.R.B., Barkhof, F., Scheltens, P., Stam, C.J., Smith, S.M., Beckmann, C.F., 2006. Consistent resting-state networks across healthy subjects. *Proc. Nat. Acad. Sci. U.S.A.* 103 (37), 13848–13853. doi:10.1073/pnas.0601417103.
- Donoghue, T., Haller, M., Peterson, E.J., Varma, P., Sebastian, P., Gao, R., Noto, T., Lara, A.H., Wallis, J.D., Knight, R.T., Shestuyuk, A., Voytek, B., 2020. Parameterizing neural power spectra into periodic and aperiodic components. *Nat. Neurosci.* 23 (12), 1655–1665. doi:10.1038/s41593-020-00744-x.
- Donoghue, T., Schaworonkow, N., Voytek, B., 2021. Methodological considerations for studying neural oscillations. *Eur. J. Neurosci.* 1–26. doi:10.1111/ejn.15361.
- Eickhoff, S.B., Yeo, B.T.T., Genov, S., 2018. Imaging-based parcellations of the human brain. *Nat. Rev. Neurosci.* 19 (11), 672–686. doi:10.1038/s41583-018-0071-7.
- Fanselow, M.S., Dong, H., 2010. Are The Dorsal and Ventral Hippocampus functionally distinct structures? *Neuron* 65 (1), 7–19. doi:10.1016/j.neuron.2009.11.031.
- Ferrarelli, F., Sarasso, S., Guller, Y., Riedner, B.A., Peterson, M.J., Bellesi, M., Massimini, M., Postle, B.R., Tononi, G., 2012. Reduced natural oscillatory frequency of frontal thalamocortical circuits in schizophrenia. *Arch. Gen. Psychiatry* 69 (8), 766–774. doi:10.1001/archgenpsychiatry.2012.147.
- Fransson, P., Marrelec, G., 2008. The precuneus/posterior cingulate cortex plays a pivotal role in the default mode network: Evidence from a partial correlation network analysis. *Neuroimage* 42 (3), 1178–1184. doi:10.1016/j.neuroimage.2008.05.059.
- Frauscher, B., Von Ellenrieder, N., Zelmann, R., Doležalová, I., Minotti, L., Olivier, A., Hall, J., Hoffmann, D., Nguyen, D.K., Kahane, P., Dubeau, F., Gotman, J., 2018. Atlas of the normal intracranial electroencephalogram: Neurophysiological awake activity in different cortical areas. *Brain* 141 (4), 1130–1144. doi:10.1093/brain/awy035.

- Fries, P., 2015. Rhythms for Cognition: Communication through Coherence. *Neuron* 88 (1), 220–235. doi:10.1016/j.neuron.2015.09.034.
- Gartner, M., Grimm, S., Bajbouj, M., 2015. Frontal midline theta oscillations during mental arithmetic: Effects of stress. *Frontiers in Behavioral Neuroscience* 9 (APR), 1–8. doi:10.3389/fnbeh.2015.00096.
- Gevins, A., Smith, M.E., McEvoy, L., Yu, D., 1997. High-resolution EEG mapping of cortical activation related to working memory: Effects of task difficulty, type of processing, and practice. *Cereb. Cortex* 7 (4), 374–385. doi:10.1093/cercor/7.4.374.
- Groppe, D.M., Bickel, S., Keller, C.J., Jain, S.K., Hwang, S.T., Harden, C., Mehta, A.D., 2013. Dominant frequencies of resting human brain activity as measured by the electrocorticogram. *Neuroimage* 79 (1), 223–233. doi:10.1016/j.neuroimage.2013.04.044.
- Haegens, S., Barczak, A., Musacchia, G., Lipton, M.L., Mehta, A.D., Lakatos, P., Schroeder, C.E., 2015. Laminar profile and physiology of the α rhythm in primary visual, auditory, and somatosensory regions of neocortex. *J. Neurosci.* 35 (42), 14341–14352. doi:10.1523/JNEUROSCI.0600-15.2015.
- Hari, R., Salmelin, R., Mäkelä, J.P., Salenius, S., Helle, M., 1997. Magnetoencephalographic cortical rhythms. *Int. J. Psychophysiol.* 26 (1–3), 51–62. doi:10.1016/S0167-8760(97)00755-1.
- Hari, R., Salmelin, R., 1997. Human cortical oscillations: A neuromagnetic view through the skull. *Trends Neurosci.* 20 (1), 44–49. doi:10.1016/S0166-2236(96)10065-5.
- Herweg, N.A., Solomon, E.A., Kahana, M.J., 2020. Theta Oscillations in Human Memory. *Trends Cogn. Sci.* 24 (3), 208–227. doi:10.1016/j.tics.2019.12.006.
- Hillebrand, A., Barnes, G.R., Bosboom, J.L., Berendse, H.W., Stam, C.J., 2012. Frequency-dependent functional connectivity within resting-state networks: An atlas-based MEG beamformer solution. *Neuroimage* 59 (4), 3909–3921. doi:10.1016/j.neuroimage.2011.11.005.
- Hindriks, R., Micheli, C., Mantini, D., Deco, G., 2017. Human resting-state electrophysiological networks in the alpha frequency band: Evidence from magnetoencephalographic source imaging. *BioRxiv* doi:10.1101/142091.
- Jacobs, J., 2014. Hippocampal theta oscillations are slower in humans than in rodents: Implications for models of spatial navigation and memory. *Philosophical Transactions of the Royal Society B: Biological Sciences* (1635) 369. doi:10.1098/rstb.2013.0304.
- Jasper, H., Penfield, W., 1949. Electroencephalograms in man: Effect of voluntary movement upon the electrical activity of the precentral gyrus. *Archiv Für Psychiatrie Und Nervenkrankheiten* 183, 163–174. doi:10.1007/BF01062488.
- Kalamangalam, G.P., Long, S., Chelaru, M.I., 2020. A neurophysiological brain map: Spectral parameterization of the human intracranial electroencephalogram. *Clin. Neurophysiol.* 131 (3), 665–675. doi:10.1016/j.clinph.2019.11.061.
- Keitel, A., Gross, J., 2016. Individual Human Brain Areas Can Be Identified from Their Characteristic Spectral Activation Fingerprints. *PLoS Biol.* 14 (6), 1–22. doi:10.1371/journal.pbio.1002498.
- Koechlin, E., Summerfield, C., 2007. An information theoretical approach to prefrontal executive function. *Trends Cogn. Sci.* 11 (6), 229–235. doi:10.1016/j.tics.2007.04.005.
- Lega, B.C., Jacobs, J., Kahana, M., 2012. Human hippocampal theta oscillations and the formation of episodic memories. *Hippocampus* 22 (4), 748–761. doi:10.1002/hipo.20937.
- Lehtela, L., Salmelin, R., Hari, R., 1997. Evidence for reactive magnetic 10-Hz rhythm in the human auditory cortex. *Neurosci. Lett.* 222 (2), 111–114. doi:10.1016/S0304-3940(97)13361-4.
- Leske, S., Dalal, S.S., 2019. Reducing power line noise in EEG and MEG data via spectrum interpolation. *Neuroimage* 189, 763–776. doi:10.1016/j.neuroimage.2019.01.026.
- Lew, B.J., Fitzgerald, E.E., Ott, L.R., Penhale, S.H., Wilson, T.W., 2021. Three-year reliability of MEG resting-state oscillatory power. *Neuroimage* 243, 118516. doi:10.1016/j.neuroimage.2021.118516.
- Lopes da Silva, F., 2013. EEG and MEG: Relevance to neuroscience. *Neuron* 80 (5), 1112–1128. doi:10.1016/j.neuron.2013.10.017.
- Mahjoory, K., Schoffelen, J.M., Keitel, A., Gross, J., 2020. The frequency gradient of human resting-state brain oscillations follows cortical hierarchies. *ELife* 9, 1–18. doi:10.7554/ELIFE.53715.
- Massimini, M., Huber, R., Ferrarelli, F., Hill, S., Tononi, G., 2004. The sleep slow oscillation as a traveling wave. *J. Neurosci.* 24 (31), 6862–6870. doi:10.1523/JNEUROSCI.1318-04.2004.
- Mellem, M.S., Wohltjen, S., Gotts, S.J., Ghuman, A.S., Martin, A., 2017. Intrinsic frequency biases and profiles across human cortex. *J. Neurophysiol.* 118 (5), 2853–2864. doi:10.1152/jn.00061.2017.
- Muthukumaraswamy, S.D., 2013. High-frequency brain activity and muscle artifacts in MEG/EEG: A review and recommendations. *Frontiers in Human Neuroscience* 7. doi:10.3389/fnhum.2013.00138.
- Niso, G., Rogers, C., Moreau, J.T., Chen, L.Y., Madjar, C., Das, S., Bock, E., Tadel, F., Evans, A.C., Jolicoeur, P., Baillet, S., 2016. OMEGA: The Open MEG Archive. *Neuroimage* 124, 1182–1187. doi:10.1016/j.neuroimage.2015.04.028.
- Niso, G., Tadel, F., Bock, E., Cousineau, M., Santos, A., Baillet, S., 2019. Brainstorm pipeline analysis of resting-state data from the open MEG archive. *Frontiers in neuroscience* 13, 284. doi:10.3389/fnins.2019.00284.
- Nolte, G., 2003. The magnetic lead field theorem in the quasi-static approximation and its use for magnetoencephalography forward calculation in realistic volume conductors. *Phys. Med. Biol.* 48 (22), 3637–3652. doi:10.1088/0031-9155/48/22/002.
- Onton, J., Delorme, A., Makeig, S., 2005. Frontal midline EEG dynamics during working memory. *Neuroimage* 27 (2), 341–356. doi:10.1016/j.neuroimage.2005.04.014.
- Oostenveld, R., Fries, P., Maris, E., Schoffelen, J.M., 2011. FieldTrip: Open source software for advanced analysis of MEG, EEG, and invasive electrophysiological data. *Computational Intelligence and Neuroscience* doi:10.1155/2011/156869, 2011.
- Palva, J.M., Palva, S., 2018. Functional integration across oscillation frequencies by cross-frequency phase synchronization. *Eur. J. Neurosci.* 48 (7), 2399–2406. doi:10.1111/ejn.13767.
- Raichle, M.E., MacLeod, A.M., Snyder, A.Z., Powers, W.J., Gusnard, D.A., Shulman, G.L., 2001. A default mode of brain function. *Proc. Natl. Acad. Sci.* 98 (2), 676–682. doi:10.1073/pnas.98.2.676.
- Ramkumar, P., Parkkonen, L., Hyvärinen, A., 2014. Group-level spatial independent component analysis of Fourier envelopes of resting-state MEG data. *Neuroimage* 86, 480–491. doi:10.1016/j.neuroimage.2013.10.032.
- Roopun, A.K., Kramer, M.A., Carracedo, L.M., Kaiser, M., Davies, C.H., Traub, R.D., Kopell, N.J., Whittington, M.A., 2008. Temporal interactions between cortical rhythms. *Front. Neurosci.* 2 (2), 145–154. doi:10.3389/neuro.01.034.2008.
- Rosanova, M., Casali, A., Bellina, V., Resta, F., Mariotti, M., Massimini, M., 2009. Natural frequencies of human corticothalamic circuits. *J. Neurosci.* 29 (24), 7679–7685. doi:10.1523/JNEUROSCI.0445-09.2009.
- Salmelin, R., Hari, R., 1994. Characterization of spontaneous MEG rhythms in healthy adults. *Electroencephalogr. Clin. Neurophysiol.* 91 (4), 237–248. doi:10.1016/0013-4694(94)90187-2.
- Scheeringa, R., Bastiaansen, M.C.M., Petersson, K.M., Oostenveld, R., Norris, D.G., Hagoort, P., 2008. Frontal theta EEG activity correlates negatively with the default mode network in resting state. *Int. J. Psychophysiol.* 67 (3), 242–251. doi:10.1016/j.ijpsycho.2007.05.017.
- Siegel, M., Donner, T.H., Engel, A.K., 2012. Spectral fingerprints of large-scale neuronal interactions. *Nat. Rev. Neurosci.* 13 (2), 121–134. doi:10.1038/nrn3137.
- Tiihonen, J., Hari, R., Kajola, M., Karhu, J., Ahlfors, S., Tassari, S., 1991. Magnetoencephalographic 10-Hz rhythm from the human auditory cortex. *Neurosci. Lett.* 129 (2), 303–305. doi:10.1016/0304-3940(91)90486-D.
- Tiihonen, J., Kajola, M., Hari, R., 1989. Magnetic Mu rhythm in man. *Neuroscience* 32 (3), 793–800. doi:10.1016/0306-4522(89)90299-6.
- Tzourio-Mazoyer, N., Landeau, B., Papathanassiou, D., Crivello, F., Etard, O., Delcroix, N., Mazoyer, B., Joliot, M., 2002. Automated anatomical labeling of activations in SPM using a macroscopic anatomical parcellation of the MNI MRI single-subject brain. *Neuroimage* 15 (1), 273–289. doi:10.1006/nimg.2001.0978.
- Van Veen, B.D., Van Drongelen, W., Yuchtman, M., Suzuki, A., 1997. Localization of brain electrical activity via linearly constrained minimum variance spatial filtering. *IEEE Trans. Biomed. Eng.* 44 (9), 867–880. doi:10.1109/10.623056.
- Varela, F., Lachaux, J.P., Rodriguez, E., Martinerie, J., 2001. The brainweb: Phase synchronization and large-scale integration. *Nat. Rev. Neurosci.* 2 (4), 229–239. doi:10.1038/35067550.
- Vidaurre, D., Hunt, L.T., Quinn, A.J., Hunt, B.A.E., Brookes, M.J., Nobre, A.C., Woolrich, M.W., 2018. Spontaneous cortical activity transiently organizes into frequency specific phase-coupling networks. *Nat. Commun.* 9 (1). doi:10.1038/s41467-018-05316-z.
- Watrous, A.J., Tandon, N., Conner, C.R., Pieters, T., Ekstrom, A.D., 2013. Frequency-specific network connectivity increases underlie accurate spatiotemporal memory retrieval. *Nat. Neurosci.* 16 (3), 349–356. doi:10.1038/nn.3315.
- Whitham, E.M., Pope, K.J., Fitzgibbon, S.P., Lewis, T., Clark, C.R., Loveless, S., Broberg, M., Wallace, A., DeLosAngeles, D., Lillie, P., Hardy, A., Fronsco, R., Pulbrook, A., Willoughby, J.O., 2007. Scalp electrical recording during paralysis: quantitative evidence that EEG frequencies above 20 Hz are contaminated by EMG. *Clin. Neurophysiol.* 118 (8), 1877–1888. doi:10.1016/j.clinph.2007.04.027.
- Yeo, B.T.T., Krienen, F.M., Sepulcre, J., Sabuncu, M.R., Lashkari, D., Hollinshead, M., Roffman, J.L., Smoller, J.W., Zöllei, J., Polimeni, J.R., Fisch, B., Liu, H., Buckner, R.L., 2011. The organization of the human cerebral cortex estimated by intrinsic functional connectivity. *J. Neurophysiol.* 106 (3), 1125–1165. doi:10.1152/jn.00338.2011.
- Zeidman, 2016. Episodic Memory. In: *International Encyclopedia of the Social & Behavioral Sciences: Second Edition*, 3. Elsevier, pp. 856–861. doi:10.1016/B978-0-08-097086-8.51032-0.
- Zuure, M.B., Hinkley, L.B., Tiesinga, P.H.E., Nagarajan, S.S., Cohen, M.X., 2020. Multiple midfrontal thetas revealed by source separation of simultaneous MEG and EEG. *J. Neurosci.* 40 (40), 7702–7713. doi:10.1523/JNEUROSCI.0321-20.2020.